

SCIENTIFIC REPORTS



OPEN

Associations of Tumor PD-1 Ligands, Immunohistochemical Studies, and Textural Features in ^{18}F -FDG PET in Squamous Cell Carcinoma of the Head and Neck

Rui-Yun Chen¹, Ying-Chun Lin^{2,3}, Wei-Chih Shen⁴, Te-Chun Hsieh^{5,6}, Kuo-Yang Yen^{5,6}, Shang-Wen Chen^{2,7,8,9} & Chia-Hung Kao^{5,9,10}

To know tumor PD-L1 expression through IHC or the FDG-PET related radiomics, we investigated the association between programmed cell death protein 1 ligand (PD-L1) expression and immunohistochemical (IHC) biomarkers or textural features of ^{18}F -fluoro-2-deoxyglucose positron emission tomography (^{18}F -FDG PET) in 53 oropharyngeal or hypopharyngeal cancer patients who were ready to undergo radiotherapy-based treatment. Differences in textural features or biomarkers between tumors with and without PD-L1 expression were tested using a Mann–Whitney U test. The predicted values for PD-L1 expression were examined using logistic regression analysis. The mean percentages of tumor PD-L1 expression were 6.2 ± 13.5 . Eighteen tumors had PD-L1 expression $\geq 5\%$, whereas 30 tumors $\geq 1\%$. Using a 5% cutoff, the *p16* staining percentage and the textural index of correlation were two factors associated with PD-L1 expression. The odds ratios (ORs) were 17.00 ($p = 0.028$) and 0.009 ($p = 0.015$), respectively. When dichotomizing PD-L1 at 1%, the *p16* and *Ki-67* staining percentages were two predictors for PD-L1 expression with ORs of 11.41 ($p = 0.035$) and 757.77 ($p = 0.045$). *p16* and *Ki-67* staining percentages and several PET/CT-derived textural features can provide supplemental information to determine tumor PD-L1 expression in HNCs.

Head and neck cancer (HNC) is the fifth most common malignancy worldwide¹, with most patients presenting with locoregionally advanced disease, and more than 50% experiencing recurrence within 3 years². Advances in the understanding of the immune system's role in tumor development have led to malignant cells being recognized as having the ability to elude immune control through the deregulation of inhibitory signals or other specific immune checkpoints. A randomized trial investigating the inhibitors of programmed cell death protein 1 (PD-1) in recurrent HNC squamous cell carcinoma showed promising results³. Tumor PD-1 ligand (PD-L1) expression reflects an immune-active microenvironment; although it is associated with other immunosuppressive molecules including PD-1 and PD-L2, PD-L1 expression is the single factor most closely correlated with response to anti-PD-1 blockade⁴. Although no standardized method for PD-L1 detection or cutoff has been defined, significant associations were found between tumor PD-L1 expression, the presence of intratumoral immune cell

¹Department of Pathology, China Medical University Hospital, Taichung, Taiwan. ²Department of Radiation Oncology, China Medical University Hospital, Taichung, Taiwan. ³The Ph.D. Program for Cancer Biology and Drug Discovery, China Medical University and Academia Sinica, Taichung, Taiwan. ⁴Department of Computer Science and Information Engineering, Asia University, Taichung, Taiwan. ⁵Department of Nuclear Medicine and PET Center, China Medical University Hospital, Taichung, Taiwan. ⁶Department of Biomedical Imaging and Radiological Science, China Medical University, Taichung, Taiwan. ⁷School of Medicine, China Medical University, Taichung, Taiwan. ⁸School of Medicine, Taipei Medical University, Taipei, Taiwan. ⁹Graduate Institute of Clinical Medical Science, School of Medicine, College of Medicine, China Medical University, Taichung, Taiwan. ¹⁰Department of Bioinformatics and Medical Engineering, Asia University, Taichung, Taiwan. Rui-Yun Chen and Ying-Chun Lin contributed equally to this work. Correspondence and requests for materials should be addressed to S.-W.C. (email: vincent1680616@yahoo.com.tw) or C.-H.K. (email: d10040@mail.cmuh.org.tw)

infiltrates, and the expression of PD-1 receptor in tumor-infiltrating lymphocytes (TILs). This suggested that PD-L1 reflects an immune-reactive milieu⁴. In addition, recent data suggested that patients with tumors that overexpress PD-L1 have an increased chance of superior clinical outcomes after anti-PD-1-directed therapy⁵. To date, other than quantifying PD-L1 through immunohistochemistry (IHC), no predictors are available to identify patients with tumors that have a higher PD-L1 expression and may benefit from checkpoint inhibitors.

Among image-based modalities for noninvasive tumor assessment, positron emission tomography with 18-fluorodeoxyglucose (¹⁸F-FDG PET) remains one of the most extensively used methods in the diagnostic workup of patients with various cancers. Recently, a pilot study for nonsmall cell lung cancer showed a direct association between metabolic parameters on FDG-PET and the expression of tumor-related immunity markers, suggesting a potential role for FDG-PET in characterizing the tumor microenvironment and selecting suitable candidates as checkpoint inhibitors⁶. However, no studies have reported the correlation between metabolic information on FDG-PET and the tissue expression of PD-L1 across various cancers. Because of the intrinsically dynamic nature of immune responses, and given the hurdles of performing new tumor biopsies aimed at investigating potential molecular predictors of checkpoint inhibitor activity in pretreated HNCs, noninvasive or minimally invasive approaches to aid patient selection are warranted. Moreover, the microenvironments of cancer tissues often present with biological heterogeneity corresponding to hypoxia, angiogenesis, or immunogenicity⁷. Such biological characteristics are of interest because they are associated with radiomics⁸. To gain greater knowledge regarding the effect of a tumor microenvironment, detected through IHC or the FDG-PET related radiomics, on tumor PD-L1 expression, we conducted this study to investigate the associations between tumor PD-L1 expression, several protein biomarkers involving the pathogenesis of hypoxia, angiogenesis, and proliferation, and ¹⁸F-FDG PET-based textural features in patients with HNCs.

Materials and Methods

Study population. Between January 2007 and December 2013, we retrospectively analyzed 53 patients with newly diagnosed oropharyngeal or hypopharyngeal squamous cell carcinoma who were ready to receive definitive chemoradiotherapy or radiotherapy for organ preservation at China Medical University Hospital. All patients had undergone pretreatment ¹⁸F-FDG PET-computed tomography (PET/CT) for staging. All patients had normal serum glucose levels before undergoing PET/CT. This study was approved by a local institutional review board (CMUH103-REC2-093FR and DMR99-IRB-010-1). The IRB also specifically waived the consent requirement.

Immunohistochemistry. As described previously using IHC⁹, gene expression profiles can be classified into hypoxic markers (*Glut1*, *CAIX*, *VEGF*, and *HIF-1 α*)¹⁰, radioresistant markers (*Bcl-2*, *CLAUDIN-4*, *YAP-1*, and *c-Met*)¹¹, a proliferative marker (*Ki-67*)¹², a tumor progression factor (*EGFR*)¹³, and a surrogate marker for human papillomavirus (HPV; *CDKN2A*)¹⁴. The spots of each pretreatment incisional biopsy were microscopically selected and arranged pairwise in tissue microarray blocks. Each tumor was represented by one tissue core on a tissue microarray. Furthermore, 4- μ m-thick paraffin sections were deparaffinized and microwaved according to standard procedures before being processed for IHC staining.

Tissue slides were scored by two pathologists blinded to the study endpoints, and any disagreement between the two observers was resolved through consensus. This was because data dichotomization in IHC studies could distort the exact correlation between the study endpoints and protein biomarkers. Continuous scoring of the biomarkers using an H-score were reported, which was derived through a summation of the percentage of area stained at each intensity level multiplied by the weighted intensity. As detailed previously⁹, nuclear staining was performed for *HIF-1 α* and *Ki-67*, whereas only cell membrane staining was performed for *EGFR*, *CAIX*, *c-Met*, *Claudin-4*, and *Glut-1*. *VEGF* and *Bcl-2* exhibited a membranous or cytoplasmic staining pattern. *YAP-1* was visualized through cytoplasmic or nuclear staining.

PD-L1 expression detected through IHC. Tumor PD-L1 biomarker was evaluated through IHC staining using DAKO clone 22C3 pharmDx (DAKO, Carpinteria, CA). Formalin-fixed paraffin embedded tumor tissues were deparaffinized and dehydrated in xylene and graded ethanol solutions. PD-L1 expressions were scored according to a tumor proportion score, which was defined as the percentage of tumor cells with complete or partial membranous staining at any intensity^{15,16}. Representative images of IHC staining for PD-L1 are illustrated in Appendix 1.

HPV status determination using p16 as a marker. In this study, *p16* overexpression detected through IHC staining was considered a surrogate marker for HPV involvement, which was verified in ten patients through the detection of HPV DNA using chromogenic *in situ* hybridization and polymerase chain reaction. Moreover, *p16* expression was scored as positive when strong and diffuse nuclear and cytoplasmic staining was present in $\geq 70\%$ of tumor cells¹⁴. Representative images of *p16* positive cells are illustrated in Appendix 2. Fourteen patients (26%) were identified as having HPV-associated cancers. Tumors originated in the oropharynx and hypopharynx in 30 and 23 patients, respectively. The median age of the patients was 51 years. We performed tumor staging according to the American Joint Committee on Cancer criteria and observed that 7 and 46 patients had stage III and IVA-IVB cancer, respectively. Patient characteristics are listed in Table 1.

PET/CT imaging. All patients were scanned using a PET/CT scanner (PET/CT-16 slice, Discovery STE; GE Medical System, Milwaukee, WI, USA). The patients were requested to fast for at least 4 hours before the administration of (¹⁸F)-FDG, and FDG PET/CT imaging was conducted approximately 60 minutes after the administration of 370 MBq of ¹⁸F-FDG. Thus, FDG uptake was determined in order to calculate the standardized uptake value (SUV). The maximum SUV (SUV_{max}) was confirmed through consensus between two nuclear medicine physicians.

In addition, the CT-based gross tumor volume was obtained for all patients as previously described⁹.

Variables	Value
Age (year)	median 53 (range, 32 ~ 75)
Gender	Male: 53
Primary tumor site	
oropharynx	30 (57%)
hypopharynx	23 (43%)
T stage	
T1	1(2%)
T2	22 (41%)
T3	18 (34%)
T4	12 (23%)
AJCC stage	
III	7 (13%)
IVA	46 (87%)
Histology grade of squamous cell carcinoma	
well differentiated	14 (26%)
moderately differentiated	17(32%)
poorly differentiated	11 (21%)
unclassified	11 (21%)
Smoking	
smoker	45(85%)
never-smoker	8(15%)
Betel nut squid	
yes	41(77%)
never	12 (23%)
Alcohol drinking	
alcoholism	36 (68%)
non-alcoholism	17 (32%)
HPV status	
p16 expression $\geq 70\%$	14 (26%)
p16 expression $< 70\%$	39 (74%)
SUVmax	mean 10.1 \pm 4.8 (range, 2.3~ 24.1)
CT-based tumor volume (ml)	mean 32.8 \pm 33.7 (range, 3 ~ 375)

Table 1. Patients' characteristics (N = 53). AJCC = American Joint Committee on Cancer criteria.

Calculation of textural indices. The metabolic tumor volume (MTV) of a tumor was delineated through an adaptive threshold method using a signal to background ratio. A voxel was defined as a local maximum if its SUV was not smaller than those of its neighbors. The SUV_{max} of a tumor was the local maximum with the largest SUV within the spatial extent. All voxels with an SUV greater than $SUV_{max} \times 0.7$ that were connected to the SUV_{max} were grouped to form a temporary MTV of the tumor. Similarly, the local maximum located outside of the temporary MTV with the shortest distance was identified and used to delineate a background MTV in the same manner. The average SUV of the temporary MTV, SUV_{mean} , and that of the background MTV, SUV_{BKG} , were calculated and used to define an adaptive threshold as follows:

$$\text{Threshold} = \beta \text{SUV}_{mean} + \text{SUV}_{BKG}$$

where $\beta = 0.15^{17}$. Finally, the MTV of the tumor was delineated using the threshold.

The heterogeneity of a tumor was evaluated using its textural features. The SUVs within a tumor were discretized using fixed bin widths of 0.05, 0.1, 0.2, 0.25, and 0.5 g/mL. For each discretization, four matrices were calculated to describe the texture of SUVs within the tumor: the gray-level co-occurrence matrix (GLCM)¹⁸, neighboring gray-level dependence matrix¹⁹, gray-level run length matrix (GLRLM)²⁰, and gray-level size zone matrix (GLSZM)²¹. Because the definitions of GLCM and GLRLM are directional, 13 matrices were calculated for all possible orientation settings for each matrix. Finally, the textural features defined for each matrix were calculated. In total, 41 textural features or histograms were extracted (Appendix 3). The features were adopted on the basis of their ability to predict local recurrence after definitive radiotherapy or chemoradiotherapy, as previously described⁸.

Statistical analysis. Correlations between PD-L1 expression and different IHC studies or textural features were examined using Spearman's rank correlation coefficient, with the alpha level set at 0.01. To compare their predictive ability for PD-L1 expression, all of the extracted features were first examined through receiver-operating characteristic (ROC) curve analysis using the aforementioned discretization methods. The

Classification of matrix	Index	AUC/ <i>p</i> value cutoff 5%	AUC/ <i>p</i> value cutoff 1%
Immunohistochemical biomarker	<i>Ki-67</i>	0.69 ± 0.07/0.024	0.72 ± 0.07/0.006
	<i>p16</i>	0.72 ± 0.07/0.011	0.75 ± 0.07/0.002
Conventional PET-related parameter	SUV _{max}	0.50 ± 0.09/0.98	0.66 ± 0.08/0.05
	MTV	0.28 ± 0.07/0.009	0.45 ± 0.08/0.53
	TLG _{mean}	0.32 ± 0.08/0.035	0.52 ± 0.08/0.79
Gray Level Cooccurrence Matrix (GLCM)	correlation	0.24 ± 0.07/0.002	0.45 ± 0.08/0.53
	energy	0.69 ± 0.08/0.035	0.56 ± 0.08/0.48
	entropy	0.31 ± 0.08/0.029	0.46 ± 0.08/0.58
Gray-Level Run Length Matrix (GLRLM)	SRE	0.71 ± 0.07/0.011	0.56 ± 0.08/0.45
	LRE	0.29 ± 0.07/0.011	0.43 ± 0.08/0.40
	GLN _{Ur}	0.28 ± 0.08/0.011	0.41 ± 0.08/0.25
	RP	0.29 ± 0.07/0.011	0.39 ± 0.08/0.18
	RLNU	0.30 ± 0.08/0.017	0.46 ± 0.08/0.66
Neighborhood Gray-Level Different Matrix (NGLDM)	coarseness	0.68 ± 0.08/0.038	0.51 ± 0.08/0.89
	contrast	0.70 ± 0.08/0.021	0.61 ± 0.08/0.20
Gray-Level Zone Length Matrix (GLSZM)	GLN _{Uz}	0.28 ± 0.07/0.011	0.45 ± 0.08/0.54
	ZLNU	0.33 ± 0.08/0.044	0.52 ± 0.08/0.84
	SZLGE	0.35 ± 0.08/0.08	0.31 ± 0.07/0.018

Table 2. Predictive abilities of biomarkers or textural indices for PD-L1 expression according to 1% and 5% cutoffs. SRE = short-run emphasis; LRE = long-run emphasis; LGRE = low gray-level run emphasis; HGRE = high gray-level run emphasis; SRLGE = short-run low gray-level emphasis; SRHGE = short-run high gray-level emphasis; LRLGE = long-run low gray-level emphasis; LRHGE = long-run high gray-level emphasis; GLN_{Ur} = gray-level nonuniformity for run; RLNU = run length nonuniformity; RP = run percentage; SZE = short-zone emphasis; LZE = long-zone emphasis; LGZE = low gray-level zone emphasis; HGZE = high gray-level zone emphasis; SZLGE = short-zone low gray-level emphasis; SZHGE = short-zone high gray-level emphasis; LZLGE = long-zone low gray-level emphasis; LZHGE = long-zone high gray-level emphasis; GLN_{Uz} = gray-level nonuniformity for zone; ZLNU = zone length nonuniformity; and ZP = zone percentage.

abilities to predict mutational status were compared through examining the area under the curve (AUC). The optimal discretization method for each feature was chosen and entered for further analysis. If the AUC for PD-L1 expression was statistically significant, the quantitative differences for these indices or IHC studies between tumors with and without PD-L1 expression were examined using a Mann–Whitney U test. Thereafter, all of the statistically significant textural indices combined with IHC parameters were tested with logistic regression analysis to seek the independent predictable factors for PD-L1 expression. All analyses were two-sided, and $p < 0.05$ was considered statistically significant. For statistically significant textural features associated with PD-L1 expression, we determined the optimal cutoff by the couple sensibility–specificity using ROC analysis. Statistical analyses were performed using SPSS, version 16.0 (SPSS Inc, Chicago, IL, USA).

Ethical approval. All procedures performed in studies involving human participants were in accordance with the ethical standards of the institutional and/or national research committee and with the 1964 Helsinki declaration and its later amendments or comparable ethical standards.

Informed consent. The IRB also specifically waived the consent requirement.

Results

Correlations between PD-L1 expression and IHC studies or textural features. The four groups of textural indices, the conventional PET-related parameters, the histograms, and the IHC staining intensities of the biomarkers were all retrieved for the entire cohort. The mean percentage of tumor PD-L1 expression was scored (6.2 ± 13.5 , range: 0–75). With different cutoffs, 12, 18, and 30 tumors had PD-L1 expressions of $\geq 10\%$, $\geq 5\%$, and $\geq 1\%$, respectively.

The PD-L1 expressions were positively correlated with *Ki-67* ($p = 0.003$, $\gamma = 0.40$), *c-Met* ($p = 0.015$, $\gamma = 0.33$), and *p16* ($p = 0.001$, $\gamma = 0.43$). The three IHC biomarkers were not related to each other (*Ki-67* and *c-Met* [$p = 0.62$, $\gamma = 0.07$], *Ki-67* and *p16* [$p = 0.08$, $\gamma = 0.25$], and *c-Met* and *p16* [$p = 0.06$, $\gamma = 0.26$]). With *p16* expression $\geq 70\%$ as a surrogate of HPV infection, the proportion of tumors having PD-L1 expressions of $\geq 5\%$ and $\geq 1\%$ was 50% and 71% in patients with HPV-positive tumors ($N = 14$) and 28% and 51% in those with HPV-negative tumors ($N = 39$).

For the various textural features, PD-L1 expression intensity was inversely correlated with gray-level nonuniformity for run (GLN_{Ur}; $p = 0.04$, $\gamma = -0.27$), run percentage (RP; $p = 0.03$, $\gamma = -0.30$), and short-zone low gray-level emphasis (SZLGE; $p = 0.04$, $\gamma = -0.28$).

In addition, the Mann–Whitney U test revealed that tumors from nonsmokers had a higher expression of PD-L1 and *p16* levels, at $p = 0.003$ and $p = 0.004$, respectively.

Variables	PD-L1 \geq 5% (N = 18)	PD-L1 < 5% (N = 35)	p value
T3-T4 tumor	9/18	21/35	0.49
Smoking	13/18	32/35	0.06
CT-based tumor volume (ml)	21.37 \pm 21.94	38.67 \pm 63.79	0.20
<i>Ki-67</i> (%)	21.33 \pm 14.95	13.51 \pm 10.81	0.005
<i>p16</i> (%)	50.28 \pm 36.56	25.91 \pm 27.38	0.002
SUVmax	10.07 \pm 4.62	10.18 \pm 4.89	0.99
MTV (ml)	7.41 \pm 10.79	92.49 \pm 429.07	0.009
TLGmean (g)	59.36 \pm 98.52	269.62 \pm 892.22	0.035
correlation (GLCM)	-0.04 \pm 0.45	0.31 \pm 0.24	0.002
energy (GLCM)	0.09 \pm 0.15	0.03 \pm 0.06	0.018
entropy (GLCM)	3.50 \pm 1.53	4.64 \pm 1.36	0.015
coarseness (NGLDM)	0.11 \pm 0.12	0.05 \pm 0.05	0.014
contrast (NGLDM)	0.26 \pm 0.65	0.20 \pm 0.95	0.021
SRE	0.98 \pm 0.04	0.94 \pm 0.06	0.01
LRE	1.09 \pm 0.14	1.28 \pm 0.36	0.01
RP	1.02 \pm 0.96	2.84 \pm 4.52	0.011
RLNU	65.35 \pm 90.67	464.92 \pm 1830.62	0.017
GLNUr	9.99 \pm 11.83	104.64 \pm 463.76	0.011
GLNUz	3.63 \pm 3.34	10.78 \pm 26.75	0.011
ZLNU	12.44 \pm 14.63	36.39 \pm 79.97	0.044

Table 3. Mann-Whitney U test for various patient-, tumor- and texture features according to tumor expression of PD-L1 \geq 5%. SRE = short-run emphasis; LRE = long-run emphasis; LGRE = low gray-level run emphasis; HGRE = high gray-level run emphasis; SRLGE = short-run low gray-level emphasis; SRHGE = short-run high gray-level emphasis; LRLGE = long-run low gray-level emphasis; LRHGE = long-run high gray-level emphasis; GLNUr = gray-level nonuniformity for run; RLNU = run length nonuniformity; RP = run percentage; SZE = short-zone emphasis; LZE = long-zone emphasis; LGZE = low gray-level zone emphasis; HGZE = high gray-level zone emphasis; SZLGE = short-zone low gray-level emphasis; SZHGE = short-zone high gray-level emphasis; LZLGE = long-zone low gray-level emphasis; LZHGE = long-zone high gray-level emphasis; GLNUz = gray-level nonuniformity for zone; ZLNU = zone length nonuniformity; and ZP = zone percentage. Note: 1. Immunohistochemical intensity and textural features are expressed as means \pm standard deviation. 2. T-stage and smoking were examined by Chi-square test.

Comparison of the predictive ability of different IHC studies and textural indices for PD-L1 expression. Because few tumors had PD-L1 expressions of \geq 10%, a binary classification of PD-L1 expression using this cutoff was excluded from the analysis. Table 2 summarizes the predictive abilities across various protein biomarkers or textural indices for PD-L1 expression using cutoffs of 1% and 5%. The ROC curves indicated that *Ki-67*, *p16*, and several textural indices were predictive of PD-L1 expressions of \geq 5%. These textural features included correlation, entropy, and energy from GLCM (26-connected and bin width = 0.1); short-run emphasis (SRE), long-run emphasis (LRE), run length nonuniformity (RLNU), GLNUr, and RP from GLRLM (26-connected and bin width = 0.5); coarseness and contrast from NGLDM (18-connected and bin width = 0.2); and gray-level nonuniformity for zone (GLNUz) and zone length nonuniformity (ZLNU) from GLSZM (18-connected and bin width = 0.5). When dichotomizing the PD-L1 expression levels at 1%, the ROC curves revealed that the good predictive performance of *Ki-67* and *p16*. However, SZLGE became a sole feature for PD-L1 expression among the indices.

The quantitative differences are listed in Table 3. The Mann-Whitney U test showed that *Ki-67*, *p16*, and 12 textural indices were predictive for PD-L1 expressions of \geq 5%. The logistic regression analysis indicated that the *p16* staining percentage and correlation from GLCM were two independent predictors for PD-L1 expression. The odds ratios (ORs) were 17.00 ($p = 0.028$; 95% confidence interval [CI]: 1.35–214.52) and 0.009 ($p = 0.015$; 95% CI: 0.00–0.41), respectively. Figure 1 depicts the quantitative difference of *p16* and correlation from GLCM between tumors with PD-L1 expressions of \geq 5% and < 5%, as well as the corresponding ROC curves. The mean percentage intensity of *p16* for tumors with PD-L1 expressions of \geq 5% and < 5% were 50.28 \pm 36.56% and 25.91 \pm 27.38%, whereas the values of correlation from GLCM were -0.04 \pm 0.45 and 0.31 \pm 0.24 for the two groups, respectively.

When dichotomizing PD-L1 expression at 1%, the logistic regression analysis revealed that the *p16* and *Ki-67* staining percentages were two predictors for PD-L1 expression. The ORs were 11.41 ($p = 0.035$; 95% CI: 1.19–109.10) and 757.77 ($p = 0.045$; 95% CI: 1.18–487860.18), respectively. The quantitative difference of the two biomarkers between tumors with PD-L1 expression of \geq 1% and < 1% are illustrated in Fig. 2. None of the PET/CT parameters or textural features were independent factors for PD-L1 expression. Smoking, tumor origin, and advanced T- or N-staging did not affect the PD-L1 expression with cutoffs of 1% or 5%.

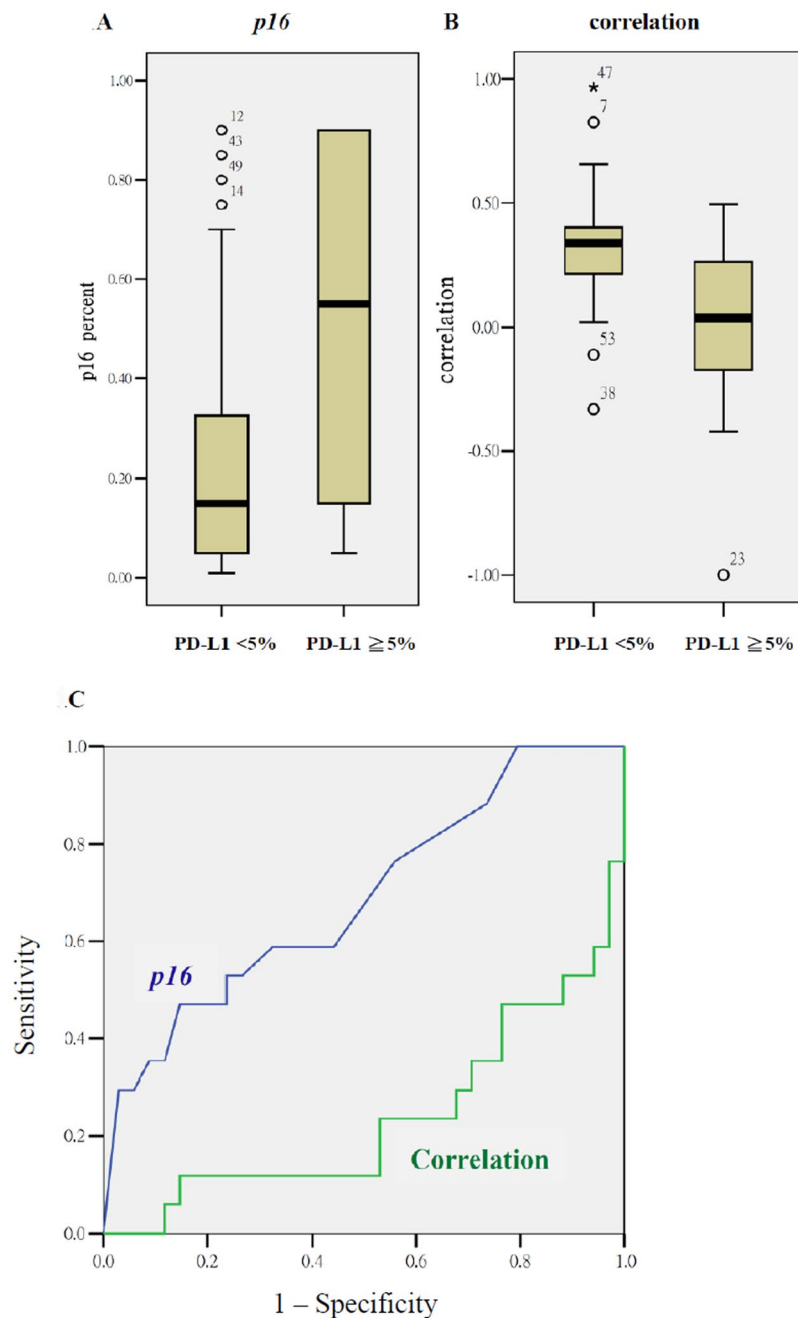


Figure 1. PD-L1 expression of $\geq 5\%$ associated with quantitative values of the IHC intensity of *p16* (1A), textural index of correlation (1B), and their ROC curves (1C). The AUCs for *p16* and the textural index of correlation were 0.72 ± 0.07 ($p = 0.011$) and 0.24 ± 0.07 ($p = 0.002$), respectively.

Accuracy in predicting PD-L1 expression. Based on the aforementioned predictive parameters, we attempted to determine the optimal cutoffs for the biomarkers to distinguish tumors above and below the cutoffs of PD-L1 expression. When a cutoff value for *p16* of 15% was chosen, the sensitivity, specificity, and accuracy for predicting PD-L1 expression of $\geq 5\%$ were 78%, 46%, and 57%, respectively. If the cutoff for PD-L1 expression was 1%, the corresponding values were 77%, 57%, and 68%, respectively.

Moreover, correlation from GLCM was a negative predictor for PD-L1 expression of $\geq 5\%$ (AUC = 0.24). When using an optimal cutoff of 0.26%, the sensitivity, specificity, and accuracy of predicting PD-L1 expression of $< 5\%$ were 66%, 67%, and 66%, respectively.

Correlation and predictive ability of IHC studies and textural features. Except for *YAP1* and *EGFR*, correlation was observed between the studied biomarkers and certain textural features (Appendix 4). Several textural features from GLCM and NGLDM were correlated well with *Claudin-4* levels, and others were related to hypoxic markers such as *VEGF* or *HIF-1 α* . Appendix 5 shows the quantitative values of textural indices that

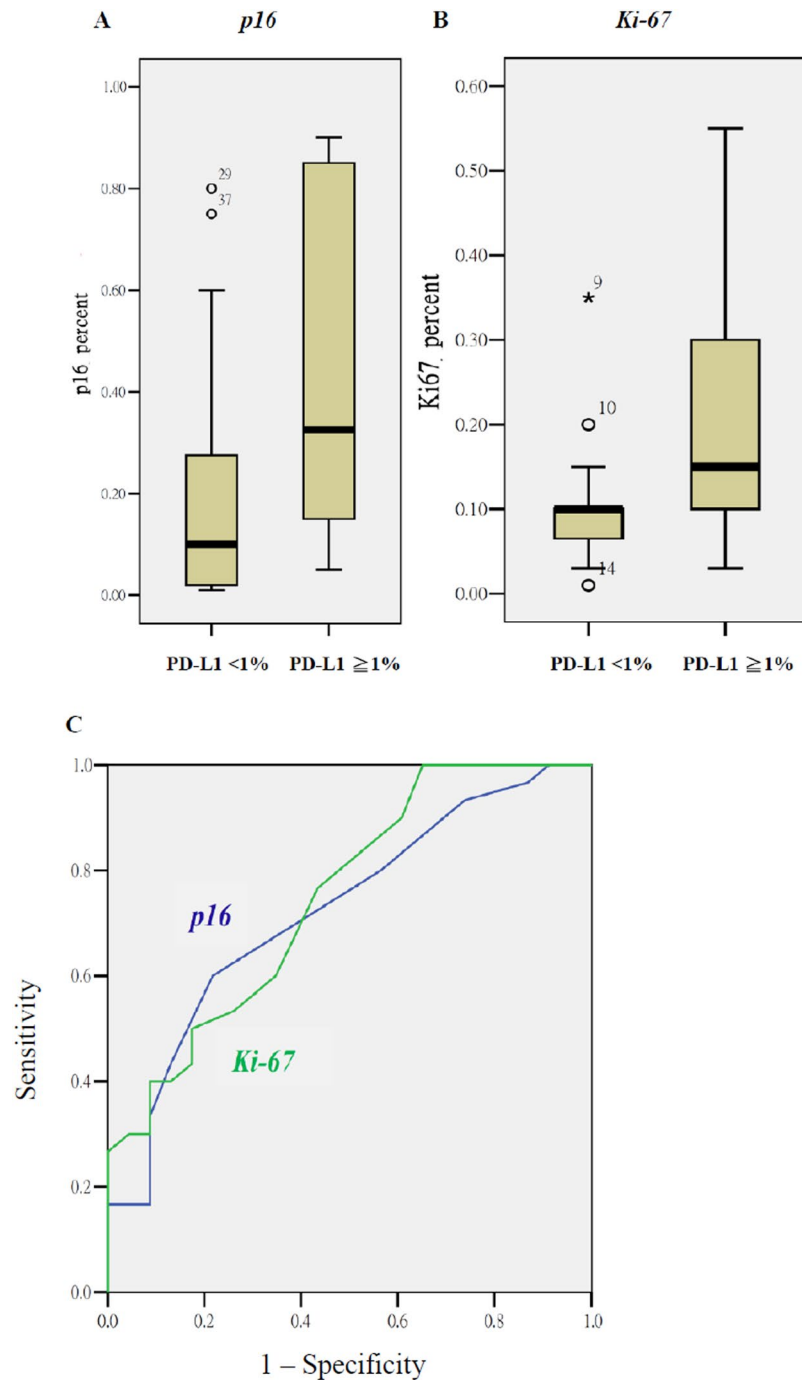


Figure 2. PD-L1 expression of $\geq 1\%$ associated with the quantitative values of the IHC intensity of *p16* (1 A), *Ki-67* (1 B), and their ROC curves (1 C). The AUCs for *p16* and the textural index of correlation were 0.75 ± 0.06 ($p = 0.002$) and 0.72 ± 0.07 ($p = 0.006$), respectively.

were associated with the intensity of biomarkers according to the 50th percentile of the IHC score, or the aforementioned optimal cutoffs⁹. In summary, the overexpression of hypoxic markers (*VEGF*, *HIF-1 α*) was positively associated with the values of entropy (GLCM), GLNUz, and RLNU. In addition, high gray-level run emphasis (HGRE), short-run high gray-level emphasis (SRHGE), high gray-level zone emphasis (HGZE), and short-zone high gray-level emphasis (SZHGE) were all positively related to *VEGF*, *Glut1*, and *Ki-67* levels, but negatively related to *Claudin-4* and *c-Met*. Furthermore, contrast (GLCM) and dissimilarity were positively associated with *VEGF* and *Glut1* levels, but negatively related to *Claudin-4* and *c-Met*. When using a cutoff of 30% for *CAIX* expression, homogeneity and variance were related to *CAIX* level.

Discussion

Immunotherapy represents a paradigm shift in cancer treatment; checkpoint inhibitors targeting the PD-1/PD-L1 axis have been reported to provide promising clinical responses in patients with various types of cancer^{5,22}. Although PD-L1 expression in numerous types of tumor has increased the chance of clinical outcomes in some cancers with anti-PD-1-directed therapy, the lack of a clear definition of positive tumor PD-L1 staining through IHC is problematic. Cutoffs for a positive result range from > 1% to > 50% based on the percentage of tumor cells stained, which suggests a connection with the existing issue of PD-L1 expression heterogeneity within the microenvironment⁵. By integrating several protein biomarkers and FDG-PET-based textural features, this pilot study revealed the association between tumor PD-L1 expression and tumor microenvironments or radiomics. Although IHC study for PD-L1 expression remains a standard care option, imaging studies or adjunctive biomarkers can provide additional information to circumvent the dynamic nature of immune microenvironments, or when timely biopsy cannot be employed.

The ratio of tumor cell PD-L1 expression in our cohort was compatible with other HNC clinical trials^{3,23}, with a positive detection rate of 20–35% obtained through IHC with a 5% cutoff. In addition, the PD-L1 expression according to HPV status was also in agreement with that of a molecular study²⁴, which reported that 70% of HPV-associated and 29% of non-HPV-associated HNCs had PD-L1 expression at the same cutoff. Theoretically, PD-L1 is biologically active only when expressed on the cell membrane, either through dynamic IFN- γ expression or constitutive oncogene activation^{5,25}. Oncogene-driven PD-L1 expression is characterized by the lack of an immune infiltrate⁴. Several studies have demonstrated the associated pathways related to oncogene activation, including *PTEN* loss^{26,27}, *EGFR* activation²⁸, and tumor hypoxia²⁹. By contrast, a positive link between tumor *p16* and PD-L1 expression in our study highlighted the model through which IFN- γ and other cytokines associated with an immune response can induce PD-L1 in tumor cells²⁴. Therefore, in patients with HPV-associated HNC, our data (as well as two other studies) suggest a rationale for the therapeutic blockade of the PD-1/PD-L1 pathway^{3,24}. Moreover, two additional studies have investigated the prognostic role of PD-L1 and other clinicopathologic features in patients with breast cancer^{30,31} and revealed that tumor PD-L1 expression is associated with an increased proliferation index of *Ki-67*. These findings were also observed in our data using the HNC cohort, although few biological studies have explored the molecular mechanism linking *Ki-67* and the PD-L1 expression pathway. Therefore, more studies across various cancers are required to clarify the biological process.

Lopci *et al.*⁶ conducted a pilot study to examine the associations between FDG-PET and the immune-active features of the tumor microenvironment. They found significant correlations between SUV_{max} and SUV_{mean} and the expressions of CD8-TILs and PD-1-TILs. However, no close relationship existed between the metabolic parameters and tumor cell PD-L1 expression. By using comprehensive FDG-PET-related textural features, the current study was the first to indicate that metabolic imaging phenotypes are able to predict tumor PD-L1 expression. To maximize predictive accuracy, a large sample size combined with machine learning processes for the selection of the discretization method may facilitate optimization of the performance of the textural features. If our findings are reproducible in additional validation studies, metabolic imaging features can be implemented to provide additional information if biopsies cannot be performed.

In addition, this study was the first to suggest that metabolic textural features from FDG-PET can indicate characteristics of some tumor microenvironments including hypoxia, angiogenesis, radioresistance, and tumor proliferation. To date, because no robust evidence exists to definitively dichotomize these protein biomarkers by differentiating treatment outcomes, we categorized them according to the 50th percentile or the optimal cutoffs reported in our previous study. In particular, several textural features were associated with tumor hypoxic markers. In oncology, identifying intratumoral areas with hypoxia is crucial because several studies on HNCs have concluded that partial oxygen pressure is one of the strongest independent predictors of overall survival, regardless of the treatment modality³². Although one study reported that there is an association between SUV_{max} of FDG and ¹⁸F-labeled nitroimidazoles (FMISO) in head and neck tumors³³, future prospective studies are required to compare FMISO and textural features of FDG to image the tumor hypoxia. Currently, little evidence exists to support a straightforward correlation between textural heterogeneity and any specific underlying physiological processes or biological heterogeneity, our findings suggest that future studies could clarify the molecular mechanisms that may be related to the interplay between imaging phenotypes and tumor microenvironments.

The findings of this study should be interpreted cautiously because of the small sample size and retrospective study design. External validation studies using an independent dataset with similar imaging and IHC studies are necessary to confirm these findings. The results would have been more robust if more immune features from tumor microenvironments, such as CD8-TILs, PD-1-TILs, and CD68 tumor-associated macrophages, were included under the scope of our analysis. However, when tumor PD-L1 expression was observed, it was frequently associated with infiltrating immune cells⁴. To elucidate the cross-talk between various immune parameters or cells, the use of larger tissue specimens instead of paraffin embedded tumor tissues is essential to recruit more immune-active markers. Furthermore, our study could not imply the correlation of FDG-PET radiomics or IHC biomarkers and the therapeutic effects with anti-PD-1 or anti-PD-L1 antibodies since the PD-L1 expression does not entirely associate with the therapeutic effects. Therefore, textural features in ¹⁸F-FDG-PET should be investigated as potential biomarkers for checkpoint inhibitors. Finally, features derived from FDG-PET-CT or IHC biomarkers remain insufficient to replace IHC testing for PD-L1 because predictive specificity and accuracy were not completely acceptable. To maximize their supplemental roles, a combination with various features or more biomarkers should be tested as a potential approach. Nonetheless, our results provide an initial step to link imaging phenotypes or IHC biomarkers and immune-active landscapes in order to maximize therapeutic strategies for checkpoint inhibitors.

Conclusion

In patients with HNC, *p16* and *Ki-67* staining percentages detected using IHC and several ¹⁸F-FDG PET/CT-derived textural features can provide supplemental information to determine tumor PD-L1 expression. The PD-L1 expressions were positively correlated with *p16* and *Ki-67*, whereas the textural index of correlation was a negative predictor for PD-L1 expression of $\geq 5\%$. Further studies are required to validate our findings and to maximize the predictive accuracy.

References

- Jemal, A. *et al.* Cancer statistics, 2009. *CA Cancer J Clin* **59**, 225–249 (2009).
- Pignon, J. P., le Maitre, A., Maillard, E. & Bourhis, J. Meta-analysis of chemotherapy in head and neck cancer (MACH-NC): an update on 93 randomised trials and 17,346 patients. *Radiother Oncol* **92**, 4–14 (2009).
- Ferris, R. L. *et al.* Nivolumab for recurrent squamous cell carcinoma of the head and neck. *N Engl J Med* **375**, 1856–1867 (2016).
- Taube, J. M. *et al.* Association of PD-1, PD-1 ligands, and other features of the tumor immune microenvironment with response to anti-PD-1 therapy. *Clin Cancer Res* **20**, 5064–74 (2014).
- Patel, S. P. & Kurzrock, R. PD-L1 Expression as a Predictive Biomarker in Cancer Immunotherapy. *Mol Cancer Ther* **14**, 847–56 (2015).
- Lopci, E. *et al.* Correlation of metabolic information on FDG-PET with tissue expression of immune markers in patients with non-small cell lung cancer (NSCLC) who are candidates for upfront surgery. *Eur J Nucl Med Mol Imaging* **43**, 1954–61 (2016).
- Hanahan, D. & Weinberg, R. A. Hallmarks of cancer: the next generation. *Cell* **144**, 646–74 (2011).
- Chen, S. W. *et al.* Correlation of pretreatment 18F-FDG PET tumor textural features with gene expression in pharyngeal cancer and implications for radiotherapy-based treatment outcomes. *Eur J Nucl Med Mol Imaging* **44**, 567–580 (2017).
- Chen, R. Y. *et al.* Immunohistochemical biomarkers and volumetric parameters for predicting radiotherapy-based outcomes in patients with p16-negative pharyngeal cancer. *Oncotarget* (2017).
- Vordermark, D. & Brown, J. M. Endogenous markers of tumor hypoxia predictors of clinical radiation resistance? *Strahlenther Onkol* **179**, 801–11 (2003).
- Akervall, J. *et al.* A novel panel of biomarkers predicts radioresistance in patients with squamous cell carcinoma of the head and neck. *Eur J Cancer* **50**, 570–81 (2014).
- Klimowicz, A. C. *et al.* The prognostic impact of a combined carbonic anhydrase IX and Ki-67 signature in oral squamous cell carcinoma. *Br J Cancer* **109**, 1859–1886 (2013).
- Kumar, B. *et al.* EGFR, p16, HPV titer, Bcl-XL and p53, sex, and smoking as indicators of response to therapy and survival in oropharyngeal cancer. *J Clin Oncol* **26**, 3128–37 (2008).
- Ang, K. K. *et al.* Human papillomavirus and survival of patients with oropharyngeal cancer. *N Engl J Med* **363**, 24–35 (2010).
- Marisa Dolled-Filhart, M. *et al.* Development of a PD-L1 immunohistochemistry (IHC) assay for use as a companion diagnostic for pembrolizumab (MK-3475) in non-small cell lung cancer (NSCLC). *J Clin Oncol* **33**, 11065–11065 (2015).
- Hutarew, G. PD-L1 testing, fit for routine evaluation? From a pathologist's point of view. *Memo* **9**, 201–206 (2016).
- Nestle, U. *et al.* Comparison of different methods for delineation of 18F-FDG PET-positive tissue for target volume definition in radiotherapy of patients with non-small cell lung cancer. *J Nucl Med* **46**, 1342–8 (2005).
- Haralick, R. M., Shanmugam, K. & Dinstein, I. Textural features for image classification. *IEEE Trans Syst Man Cybern.* **3**, 610–621 (1973).
- Sun, C. & Wee, W. G. Neighboring gray level dependence matrix for texture classification. *Comput Vis Graph Image Process.* **23**, 341–52 (1983).
- Loh, H., Leu, J. & Luo, R. The analysis of natural textures using run length features. *IEEE Trans Ind Electron.* **35**, 323–328 (1988).
- Thibault, G. *et al.* Texture indexes and gray level size zone matrix: application to cell nuclei classification. *Pattern Recognition Inf Process.* 140–145 (2009).
- Herbst, R. S. *et al.* Predictive correlates of response to the anti-PD-L1 antibody MPDL3280A in cancer patients. *Nature* **515**, 563–567 (2014).
- Grosso, J. *et al.* PD-L1 expression in various tumor types. *J Immunother Cancer* **1**, P53 (2013).
- Lyford-Pike, S. *et al.* Evidence for a role of the PD-1:PD-L1 pathway in immune resistance of HPV-associated head and neck squamous cell carcinoma. *Cancer Res* **73**, 1733–1741 (2013).
- Pardoll, D. M. The blockade of immune checkpoints in cancer immunotherapy. *Nat Rev Cancer* **12**, 252–64 (2012).
- Parsa, A. T. *et al.* Loss of tumor suppressor PTEN function increases B7-H1 expression and immunoresistance in glioma. *Nat Med* **13**, 84–8 (2007).
- Song, M. *et al.* PTEN loss increases PD-L1 protein expression and affects the correlation between PD-L1 expression and clinical parameters in colorectal cancer. *PLoS One* **8**, e65821 (2013).
- Akbay, E. A. *et al.* Activation of the PD-1 pathway contributes to immune escape in EGFR-driven lung tumors. *Cancer Discov* **3**, 1355–63 (2013).
- Barsoum, I. B., Smallwood, C. A., Siemens, D. R. & Graham, C. H. A mechanism of hypoxia-mediated escape from adaptive immunity in cancer cells. *Cancer Res* **74**, 665–74 (2014).
- Botti, G. *et al.* PD-L1 tumor expression is associated with a better prognosis and diabetic disease in triple negative breast cancer patients. *In J Mol Sci* **18**, 459 (2017).
- Muenst, S. *et al.* Expression of programmed death ligand 1 (PD-L1) is associated with poor prognosis in human breast cancer. *Breast Cancer Res Treat* **146**, 15–24 (2014).
- Brown, J. M. & William, W. R. Exploiting tumour hypoxia in cancer treatment. *Nat Rev Cancer* **4**, 437–447 (2004).
- Rajendran, J. G. *et al.* Hypoxia and Glucose Metabolism in Malignant Tumors: Evaluation by ¹⁸Fluoromisonidazole and ¹⁸Fluorodeoxyglucose Positron Emission Tomography Imaging. *Clin Cancer Res* **10**, 2245–2252 (2004).

Acknowledgements

This study is supported in part by Taiwan Ministry of Health and Welfare Clinical Trial Center (MOHW106-TDU-B-212-113004), China Medical University Hospital, Academia Sinica Taiwan Biobank Stroke Biosignature Project (BM10601010036), Taiwan Clinical Trial Consortium for Stroke (MOST 106-2321-B-039-005), Tseng-Lien Lin Foundation, Taichung, Taiwan, Taiwan Brain Disease Foundation, Taipei, Taiwan, and Katsuzo and Kiyoo Aoshima Memorial Funds, Japan. The funders had no role in study design, data collection and analysis, decision to publish, or preparation of the manuscript. No additional external funding was received for this study.

Author Contributions

All authors have contributed substantially to, and are in agreement with the content of, the manuscript: Conception/Design: Rui-Yun Chen, Ying-Chun Lin, Shang-Wen Chen, Chia-Hung Kao; Provision of study materials: Chia-Hung Kao; Collection and/or assembly of data: Rui-Yun Chen, Ying-Chun Lin, Wei-Chih Shen,

Te-Chun Hsieh, Kuo-Yang Yen, Shang-Wen Chen, Chia-Hung Kao; Data analysis and interpretation: Rui-Yun Chen, Ying-Chun Lin, Wei-Chih Shen, Te-Chun Hsieh, Kuo-Yang Yen, Shang-Wen Chen, Chia-Hung Kao; Manuscript preparation: Rui-Yun Chen, Ying-Chun Lin, Wei-Chih Shen, Te-Chun Hsieh, Kuo-Yang Yen, Shang-Wen Chen, Chia-Hung Kao; Final approval of manuscript: Rui-Yun Chen, Ying-Chun Lin, Wei-Chih Shen, Te-Chun Hsieh, Kuo-Yang Yen, Shang-Wen Chen, Chia-Hung Kao. The guarantor of the paper, taking responsibility for the integrity of the work as a whole, from inception to published article: Chia-Hung Kao.

Additional Information

Supplementary information accompanies this paper at <https://doi.org/10.1038/s41598-017-18489-2>.

Competing Interests: The authors declare that they have no competing interests.

Publisher's note: Springer Nature remains neutral with regard to jurisdictional claims in published maps and institutional affiliations.



Open Access This article is licensed under a Creative Commons Attribution 4.0 International License, which permits use, sharing, adaptation, distribution and reproduction in any medium or format, as long as you give appropriate credit to the original author(s) and the source, provide a link to the Creative Commons license, and indicate if changes were made. The images or other third party material in this article are included in the article's Creative Commons license, unless indicated otherwise in a credit line to the material. If material is not included in the article's Creative Commons license and your intended use is not permitted by statutory regulation or exceeds the permitted use, you will need to obtain permission directly from the copyright holder. To view a copy of this license, visit <http://creativecommons.org/licenses/by/4.0/>.

© The Author(s) 2017